Kovove Mater. 63 2025 169–179 DOI: 10.31577/km.2025.3.169

# Rotary friction welding of 304L-310S austenitic stainless steels

Abdeldjebar Hadji<sup>1</sup>, El-Hadj Raouache<sup>2</sup>, Zakaria Boumerzoug<sup>1</sup>\*, Fares Khalfallah<sup>3</sup>, François Brisset<sup>4</sup>, Thierry Baudin<sup>4</sup>

<sup>1</sup>LMSM, Department of Mechanical Engineering, University of Biskra, Biskra, Algeria
 <sup>2</sup>Department of Mechanical Engineering, University of Bordj Bou Arreridj, Algeria
 <sup>3</sup> Department of Physics, Faculty of Science, University of M'sila, 28000 M'sila, Algeria
 <sup>4</sup>Université Paris-Saclay, CNRS, Institut de chimie moléculaire et des matériaux d'Orsay, 91405 Orsay, France

Received 30 November 2024, received in revised form 10 September 2025, accepted 26 September 2025

#### Abstract

The objective of this study is to examine the effect of rotational speed on the microstructure, texture, and mechanical properties of joints produced by rotary friction welding of two dissimilar austenitic stainless steels (AISI 304L and AISI 310S). The choice of these two stainless steels is based on their complementary properties and industrial relevance. The study focuses on welding dissimilar stainless steels to meet industrial requirements. To achieve these objectives, optical microscopy, scanning electron microscopy equipped with energy-dispersive X-ray spectroscopy, electron backscatter diffraction, Vickers microhardness testing, and tensile testing were used to characterize the welded joints. The joining of the two dissimilar stainless steels was successfully achieved. A microstructurally uniform welded zone was obtained at the highest rotational speed. At 1400 rpm and 2000 rpm, the welded joints achieved tensile strengths of approximately 507 MPa and 500 MPa, respectively, with weld-center hardness ranging from 220 to 230 HV. EBSD analysis revealed three distinct zones in the welded joint, characterized by different grain sizes and textures. With increasing rotational speed, unlike the central zone, adjacent zones underwent grain growth while retaining the same grain orientation as the central zone.

Keywords: Rotary Friction Welding (RFW), austenitic stainless steels, microstructures, texture, mechanical properties

## 1. Introduction

Stainless steels are an important class of engineering materials widely used in various industries and environments [1]. They are complex alloys containing a minimum of 11 % Cr, plus other elements [2]. Based on their microstructure, stainless steels are classified into five categories: ferritic, austenitic, martensitic, duplex, and precipitation-hardening. Austenitic stainless steels constitute the largest class [1]. They are attractive engineering materials due to their exceptional properties, and they are widely used in chemical, mechanical, automobile, and nuclear applications, where assembly is often carried out by welding [3, 4].

Among these grades, AISI 304L and AISI 310S austenitic stainless steels are widely used. Due to its excellent mechanical and anti-corrosion properties,

AISI 304L stainless steel is used in nuclear power plants, marine environments, and chemical plants, as well as for the transportation of natural gas [5, 6]. AISI 310S stainless steel is used primarily in the petrochemical industry, nuclear power, geothermal activities and oil and gas production due to its excellent resistance to oxidation, hydrogen embrittlement, and corrosion [7]. The welded joints of AISI 304L and AISI 310S are recommended for high-temperature zones, where AISI 310S exhibits improved corrosion/oxidation resistance [8]. Additionally, these dissimilar joints (AISI 304L-AISI 310S) can be employed in petrochemical industries for catalytic reforming units, where AISI 310S provides the strength and stability required near furnaces, while AISI 304L offers cost-efficient solutions in cooler sections.

Although austenitic stainless steels are renowned

<sup>\*</sup>Corresponding author: tel.: +213 775759694; e-mail address: z.boumerzoug@univ-biskra.dz

| Material           | V               | Cr            | Mn               | Fe              | Со               | Ni             | Cu             | Mo               |
|--------------------|-----------------|---------------|------------------|-----------------|------------------|----------------|----------------|------------------|
| SS 304L<br>SS 310S | $0.08 \\ 0.107$ | 17.49 $24.04$ | $1.204 \\ 1.495$ | 72.882 $53.613$ | $0.095 \\ 0.142$ | 7.964 $20.293$ | 0.181<br>0.184 | $0.087 \\ 0.124$ |

Table 1. Chemical composition of base metals: Austenitic stainless steel 304L and 310S

for their weldability [9], welding can still be challenging due to their physical properties [10]. Traditional arc welding can result in the formation of intergranular Cr-rich carbides at grain boundaries, leading to heat-affected zone (HAZ) cracking, coarse grain growth, and creep failure [11]. Rotary friction welding (RFW) has shown promise in overcoming these welding difficulties and is a valuable method for combining dissimilar materials [11, 12].

Rotary Friction Welding (RFW) is a thermomechanical solid-state joining process predominantly used for cylindrical workpieces [13, 14]. The technique uses controlled rotational motion to generate frictional heating and plastic deformation at the interface, with one component fixed and the other spinning while axial pressure is applied to both. Once the material softens, rotation stops, and the components are consolidated under pressure, forming a strong metallurgical bond. Generally, RFW has two stages: the friction stage and the forging stage, which is very short compared to the first. It enables effective joining of dissimilar materials, including stainless steels [15–17], and is cost-effective for creative designs and technical solutions [18]. The main parameters of RFW are rotational speed, friction time, friction pressure, forging time, and forging pressure. By controlling these parameters, an excellent welded joint can be performed.

According to previously published work, there are few studies dedicated to welding dissimilar steels using RFW [19–21], particularly the welding of dissimilar stainless steels [22]. Mattie et al. [22] devoted their study to optimizing the RFW parameters for austenitic to ferritic stainless steels. They found that the forging pressure and speed have a significant influence on the total strain. Kumar et al. [23] investigated 304SS joints and reported that the welded strength and hardness were enhanced at the highest heating and upset load. A heterogeneous grain structure also developed in the welded zone. Chatha et al. [24] compared dissimilar stainless-steel welds and found that the best combination, producing a tensile strength of 3920 kgf and a Vickers microhardness of 278 HV, was discovered in the SS316-SS304 joints. Kimura et al. [25] investigated a thin-walled AISI 310S pipe. They achieved successful joints with 100 % efficiency using a 1.50 mm pipe thickness at a friction pressure of 120 MPa. However, as the thickness decreased, joining became difficult and was not successful at a pipe thickness of 0.50 mm. Wang et al. [26] studied AISI 304 using EBSD and revealed that dynamic recrystallization (DRX) is primarily produced in the welding zone; they also observed a distinct shear-type texture ( $\{110\}<112>$ ) in the joint region.

However, previous studies on rotary friction welding of austenitic stainless steels remain very limited and have predominantly focused on similar [11, 24, 26] or austenitic-to-ferritic stainless-steel welds [10, 22]. No studies have focused on the specific combination of AISI 304L and AISI 310S. This represents a significant and unexplored research gap, since this combination offers a unique case study due to the considerable difference in alloying content (especially Cr and Ni) and their complementary high-temperature properties. Using optical microscopy, EBSD, hardness, and tensile strength testing, this study offers a novel investigation into the effect of rotational speed on these particular joints. These techniques present a comprehensive correlation between welding parameters, dynamic recrystallization, microstructural changes, and mechanical properties. The objective of this work is to investigate the effect of rotational speed on the microstructure, texture, and mechanical properties of AISI 304L-AISI 310S RFW joints, thereby filling an important knowledge gap and providing a basis for optimizing this welding technique.

## 2. Experimental procedure

For this study, two austenitic stainless steels, grades 304L and 310S, were selected in rod form with a diameter of 12 mm. The chemical composition of the base metals is shown in Table 1. The choice of AISI 304L and AISI 310S stainless steels for this study is rooted in their complementary properties and industrial relevance. AISI 304L is an austenitic stainless steel favored for its corrosion resistance, excellent mechanical properties, and adaptability to moderate operating temperatures. It is a material of choice in applications such as chemical plants, marine structures, and nuclear facilities, where cost-effectiveness and durability are critical [27].

In contrast, AISI 310S is an advanced austenitic stainless steel engineered for extremely high-temperature conditions. The chemical composition, characterized by elevated concentrations of chromium and nickel, offers exceptional oxidation resistance and thermal stability, making it a viable alternative to pricier superalloys in certain applications [28]. This makes it ideal for demanding applications such as super-heater

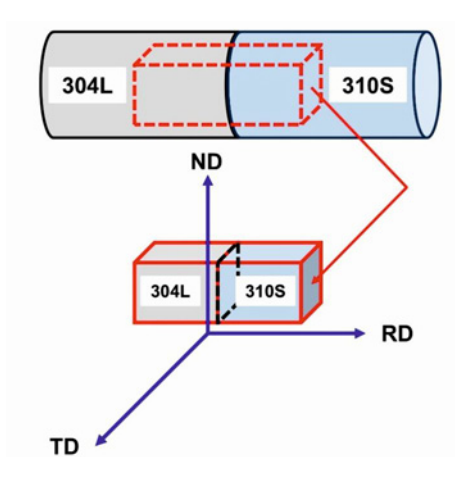


Fig. 1. Schematic representation of the weld joint with the main coordinate system: Rolling Direction (RD), Normal Direction (ND), and Transverse Direction (TD).

tubes in HRSGs, where exposure to high-temperature gas flows is prevalent, and in furnace-adjacent piping within petrochemical processes. Combining these materials in dissimilar welded joints provides a unique solution for applications with varying thermal and mechanical stresses, ensuring a balance between performance and cost-efficiency.

The machine used to carry out the RFW is a universal 3-axis vertical milling machine. RFW was performed on rods of 84 mm in length for 304L stainless steel and 89 mm for 310S steel. Before welding, the rod ends were polished and cleaned to minimize the effects of contamination. RFW was carried out by varying the rotational speed (1000, 1400, and 2000 rpm) while maintaining the other parameters constant (friction feed = 40 mm min<sup>-1</sup>, pressure = 120 MPa).

Temperature changes near the joint line were measured during welding using an infrared video thermometer (IRVT) device (FI 638TI). For microscopic observation of the welded joint, samples were cut and then polished using carbide paper (up to 1200 grains), then using polishing clothes containing a 6-micron diamond paste, and finally electrolytically etched with  $10\,\%$  oxalic acid (8V,  $60\,\mathrm{s}$ ).

For EBSD analysis, the standard sample preparation method was applied on the surface of the welded joint (ND, RD), as it is shown in the schematic representation of the welded joint (Fig. 1). The main coordinate system contains the three main directions: rolling direction (RD), transverse direction (TD), and normal direction (ND). The preparation method consists of mechanical polishing with grade 2400 emery paper, followed by OPS polishing of the surface samples. A Zeiss Supra 55 VP FEG-SEM operating at 20 kV and about 2 nA of current, coupled with OIM<sup>TM</sup> (Orientation Imaging Microscopy) software from TSL-EDAX and a Velocity camera, was used for EBSD acquisition

and analysis. The exploration step is 2  $\mu m$ . The EBSD data were analyzed, considering a grain tolerance angle of 5° and a minimum grain size of 5 pixels, on several rows. Textures were calculated using the harmonic method up to a development order of 34 and assuming a triclinic symmetry of the texture. Each orientation is modeled by a Gaussian of 5° width at half height. They are drawn in the section of the rods (so on the pole figures, the A3 axis corresponds to the Wire Axis "WA"). Furthermore, the SEM is equipped with energy dispersive spectroscopy (EDS) for chemical analysis.

Elemental analysis was carried out by energy dispersive X-ray spectroscopy (EDS) of the Bruker TES-CAN VEGA3 SBU scanning electron microscope. The tensile and hardness tests were the two mechanical tests applied to the welded samples. The tensile tests were conducted on specimens 13 cm in length, each containing a weld seam in the middle. These tests were performed on a universal Instron 8516 tensile machine equipped with a 100 kN load cell, with a tension speed of 1 mm min<sup>-1</sup>. For each welding condition (1000, 1400, and 2000 rpm), three tensile specimens were tested, and the reported values represent the average. Hardness measurements along the welded joint were carried out using a ZWICK ROELL INDEN-TEC type micro-durometer under a load of 300 g and a holding time of 10 s. Indentations were made along the midline of each welded specimen across the base metal, HAZ, TMAZ, and weld zone.

#### 3. Results and discussion

### 3.1. Macroscopic observation

Figure 2 shows the evolution of the welding procedure of the two dissimilar steel bars (the SS 310S rod is fixed, but the SS 304L rod is rotating). It is noted that under the effect of friction, the contact surface becomes increasingly red, indicating a temperature increase, which makes this area more plastic. Consequently, a bead forms at the welded joint. With the rotation of the 304L stainless-steel rod stopped (35 s), the welded joint cools gradually. The bead obtained has an almost symmetrical shape, indicating that the dissimilar steels exhibit nearly identical ductility behavior. For this welding process, the friction stage lasted 35 seconds, followed by a 10-second forging stage.

Figure 3 presents the curves of the temperature evolution of the welded joint for the three rotational speeds during RFW of 304L stainless steel to 310S stainless steel. The common point between these three curves is that they have the same appearance. These three curves exhibit an ascending part up to a maximum temperature of approximately  $525\,^{\circ}\text{C}$ , corre-

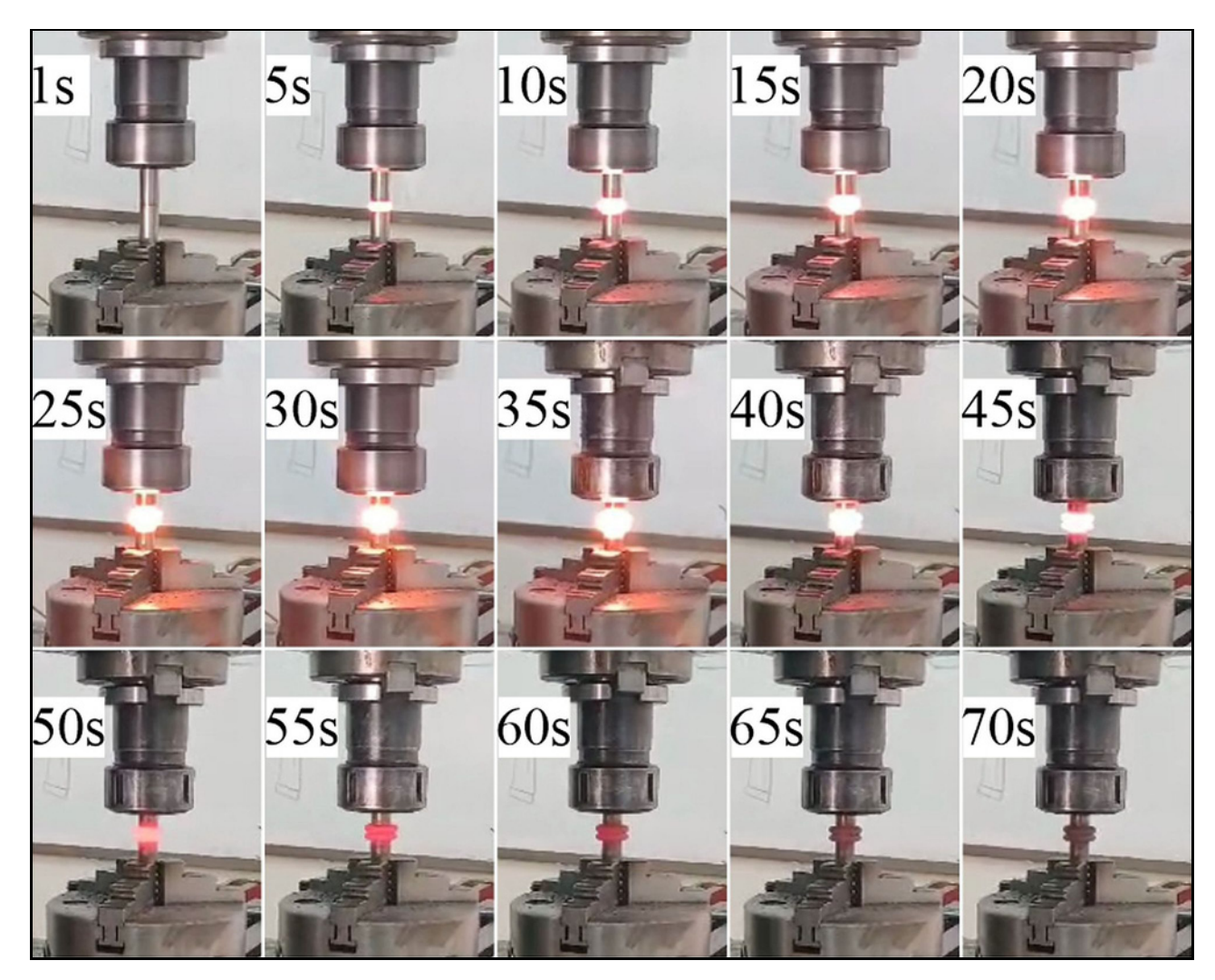


Fig. 2. Sequence of the RFW process of the two dissimilar austenitic steels.

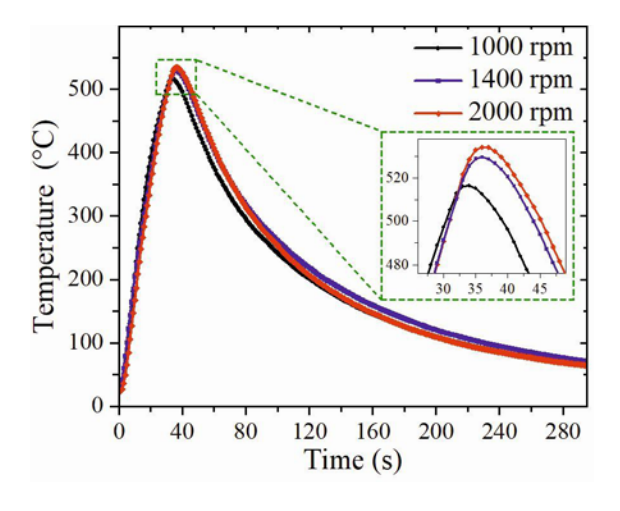


Fig. 3. Curves of the temperature evolution of the welded joint for the three rotational speeds during RFW of 304L stainless steel to 310S stainless steel.

sponding to the rapid heating during the friction stage. Then, there is a descending but somewhat slow part, which corresponds to forging, followed by the cessation of rotation. However, it was observed that at the top of the three curves, the more the rotational speed increases, the temperature also increases, meaning higher rotational speeds generate more heat at the welded joint.

## 3.2. Microstructural observation

## $3.2.1.\ Base\ metals$

Figure 4 shows the microstructure of the two base metals. The two stainless steels, 304L (Fig. 4a) and 310S (Fig. 4b), are formed from a single phase, which is austenite. It should be noted that 310S steel is composed of larger grains ( $\sim 50~\mu m)$  than 304L steel ( $\sim 10~\mu m)$ .

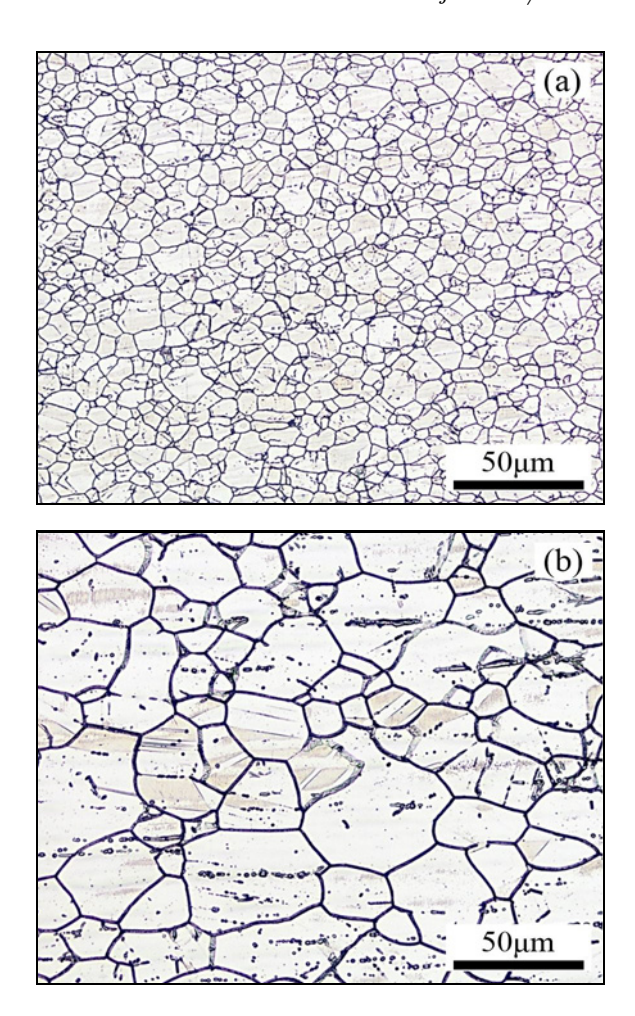
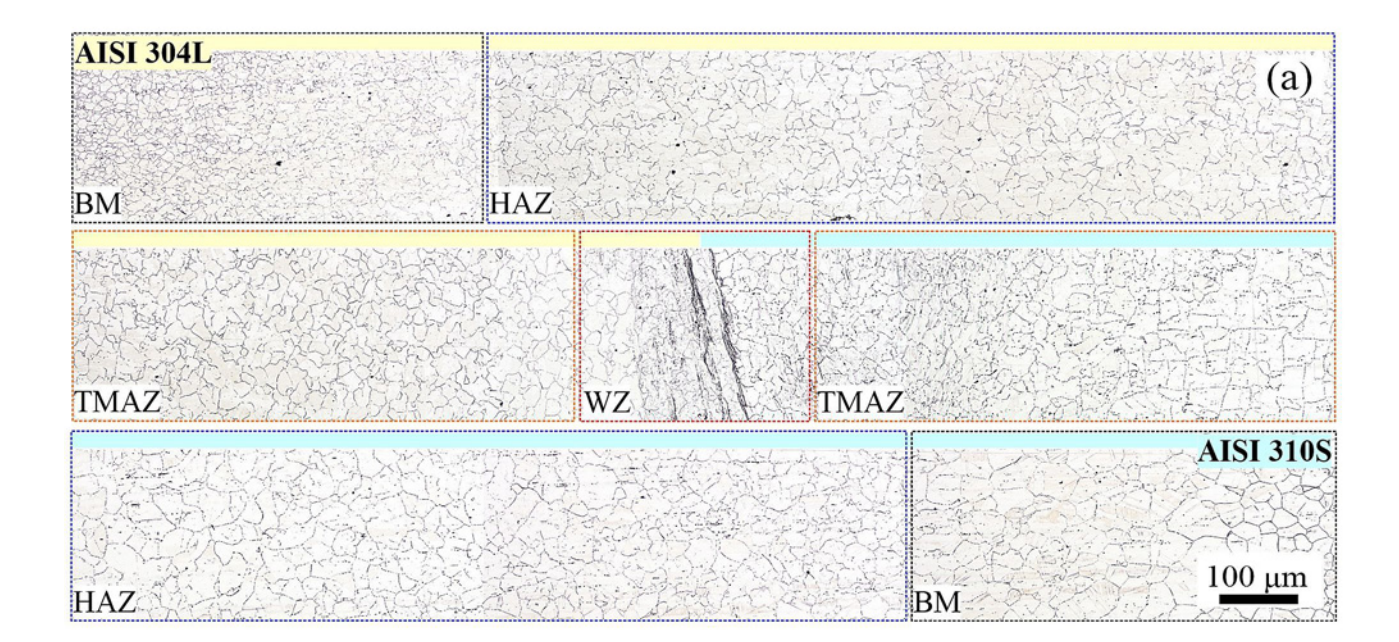


Fig. 4. Optical microstructure of: (a) Austenitic-stainless steel 304L, and (b) Austenitic-stainless steel 310S.

#### 3.2.2. Welded joints

The optical microstructures of all welded samples were examined using optical microscopy (Fig. 5). This figure presents a total view of the welded joint, allowing for the visualization of the microstructure of the different zones that typically form in a welded joint. These zones have been identified as follows: the weld zone (WZ), the thermomechanically affected zone (TMAZ), and the heat-affected zone (HAZ). These three distinct zones were observed on either side of the welded joint and are distinguished by the size of their grains. This distinction is due to the thermal and thermomechanical effects during rotary friction welding. Zhu et al. [29] measured the temperature distribution along the welded joint using RFW and an industrial infrared thermometer, showing that the temperature gradually decreases from the central point of the welded joint towards the base metal, resulting in a microstructural difference along the welded joint. For the dissimilar joint 304L/310S, the distinction between the three zones is visible for the rotational speed of 2000 rpm (Fig. 5c), where the thermomechanical contribution is greater, which influences the grain size. However, with a focused observation on the microstructure of TMAZ and the WZ, it is possible to observe two phenomena. The first phenomenon involves an increase in grain size within the TMAZ as the rotational speed increases. The second phenomenon is the formation of fine grains in the WZ. In this same zone, the deformation bands disappear at high rotational speeds (2000 rpm). By increasing the rotation speed, the microstructure on either side of the central zone will undergo grain enlargement. The central WZ zone forms small grains after being formed



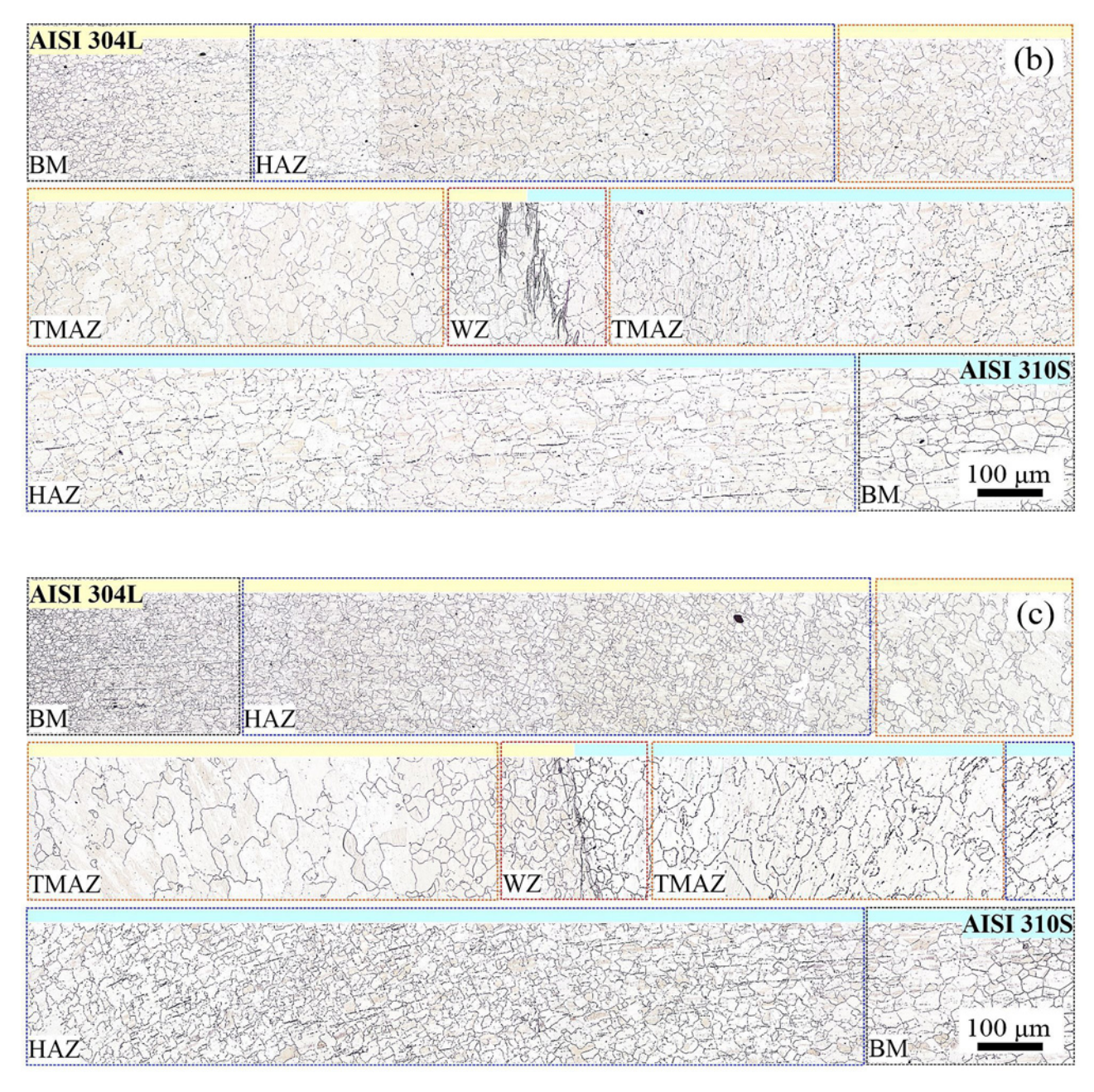


Fig. 5. Microstructures of samples welded by RFW under three rotational speeds: (a) 1000 rpm, (b) 1400 rpm, and (c) 2000 rpm.

into strong deformation bands. This phenomenon can be attributed to dynamic recrystallization. Indeed, the increase in friction heat and plastic deformation at higher speeds promotes recrystallization and grain refinement. This type of recrystallization is a dynamic recrystallization reaction, as mentioned and observed by certain authors [19, 30, 31].

## 3.4. EDS analysis

Figure 6 presents the distribution curves of the three chemical elements (Fe, Cr, and Ni) through the

welded joint for the three welded samples 1000 rpm (Fig. 6a), 1400 rpm (Fig. 6b), and 2000 rpm (Fig. 6c). Overall, the iron curve shows a remarkable difference between the two dissimilar steels, on the other hand for Cr and Ni, the difference is not significant. It is essential to note that the common feature among these three curves is the continuous variation of these chemical elements through the welded joint, indicating that welding has facilitated the diffusion of these elements, i.e., that welding by friction has not created a depleted area of these elements. The interdiffusion of certain chemical elements across the interface has been widely

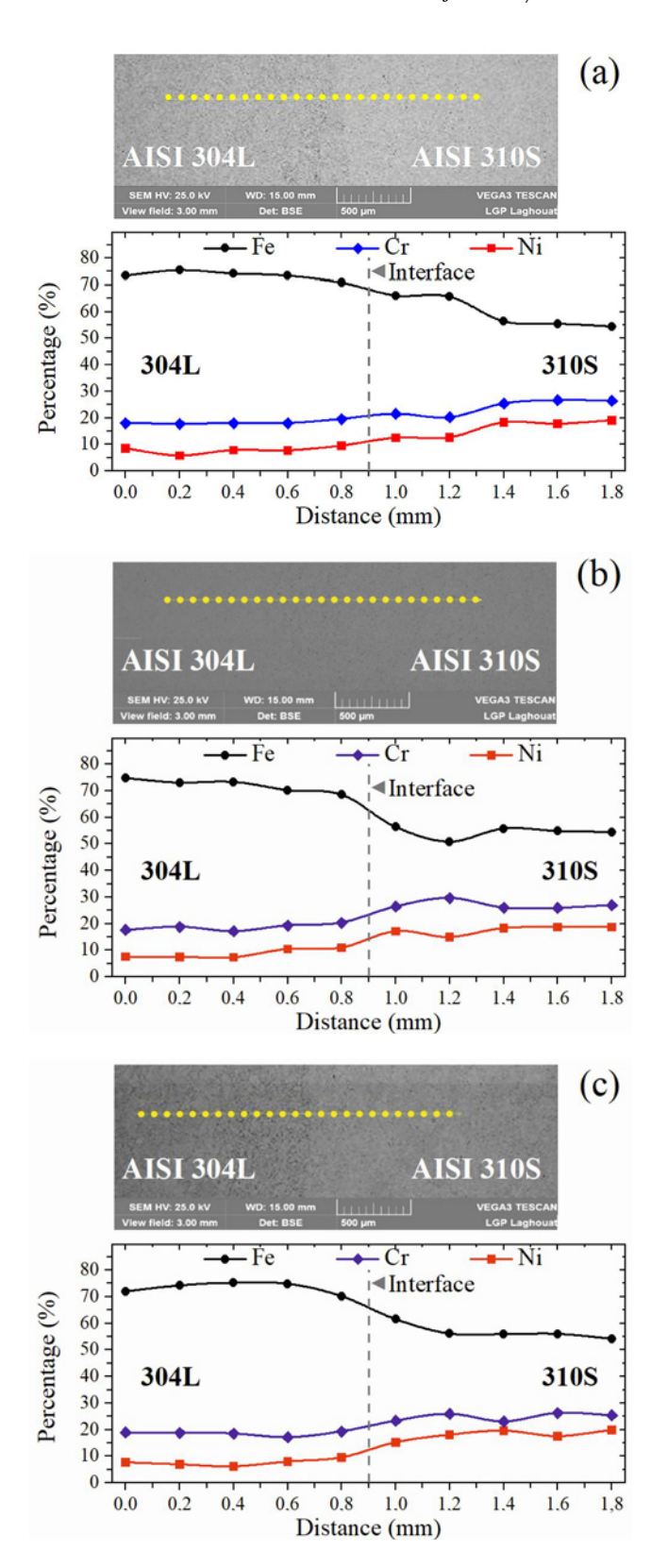


Fig. 6. Distribution curves of the three chemical elements (Fe, Cr, and Ni) through the welded joint by RFW under three rotational speeds: (a) 1000 rpm, (b) 1400 rpm, and (c) 2000 rpm.

recognized in the RFW of dissimilar materials [32-34]. However, the effect of rotational speed on the distribution of the three chemical elements is not considerable.

#### 3.5. EBSD analysis

Figure 7 shows the EBSD maps along the welded joint for the three rotational speeds (Fig. 7a), with the pole figures in the three selected zones of the welded joint (Fig. 7b). The central zone for the three welded joints is formed by small grains. This morphology is due to the intense friction effect during RFW. Wang et al. [26] investigated the microstructural evolution of AISI 304 stainless steel following rotary friction welding. The process of dynamic recrystallization (DRX) and texture formation was analyzed by optical microscope and EBSD. The results showed that dynamic recrystallization (DRX) mainly appears in the welding zone. In addition, a shear-type texture ( $\{110\}<112>$ ) is formed in the weld joint [26]. Generally, this fine microstructure contributes to the increase in hardness in this area. With the increase in rotational speed, the zone adjacent to the central zone is increasingly composed of large grains, especially at high rotational speeds (2000 rpm). This grain growth is due to the thermal effect, which increases with the increase in rotational speed. This zone is identified as the thermomechanically affected zone (TMAZ).

Concerning the pole figures (Fig. 7b) in the three selected zones of the welded joint for the three samples welded by RFW with different rotational speeds; it is worth noting that these three zones (1, 2, and 3) were selected based on the variation in grain size from one zone to another. Zone 2 generally corresponds to the welded zone and the thermo-mechanically affected zones, while zones 1 and 3 characterize the thermally affected zones.

The texture of zone 2 exhibits a pronounced texture, primarily composed of a component oriented along the {110}<112> direction at a speed of 1000 rpm. Note that the texture is not orthotropic due to the rotating friction.

With the speed of 1400 rpm, the texture of zone 2 is similar to that of the sample with the speed of 1000 rpm, except that a slight rotation of the {110}<112> component is observed, resulting in a tilting of the central pole part of the polar figure {001} towards its center. This rotation continues for 2000 rpm since an almost texture of fiber <100> // WA appears, but with all the same reinforcement of the component {001}<110>. The development of textures in a welded joint depends on the type of steel being welded and the welding process applied. For example, Priymak et al. [35] found the presence of a pronounced crystallographic texture close to that of the (110)[001] plane with the axis normal to the surface of the welded joint of medium-carbon alloy steels joined by the ro-

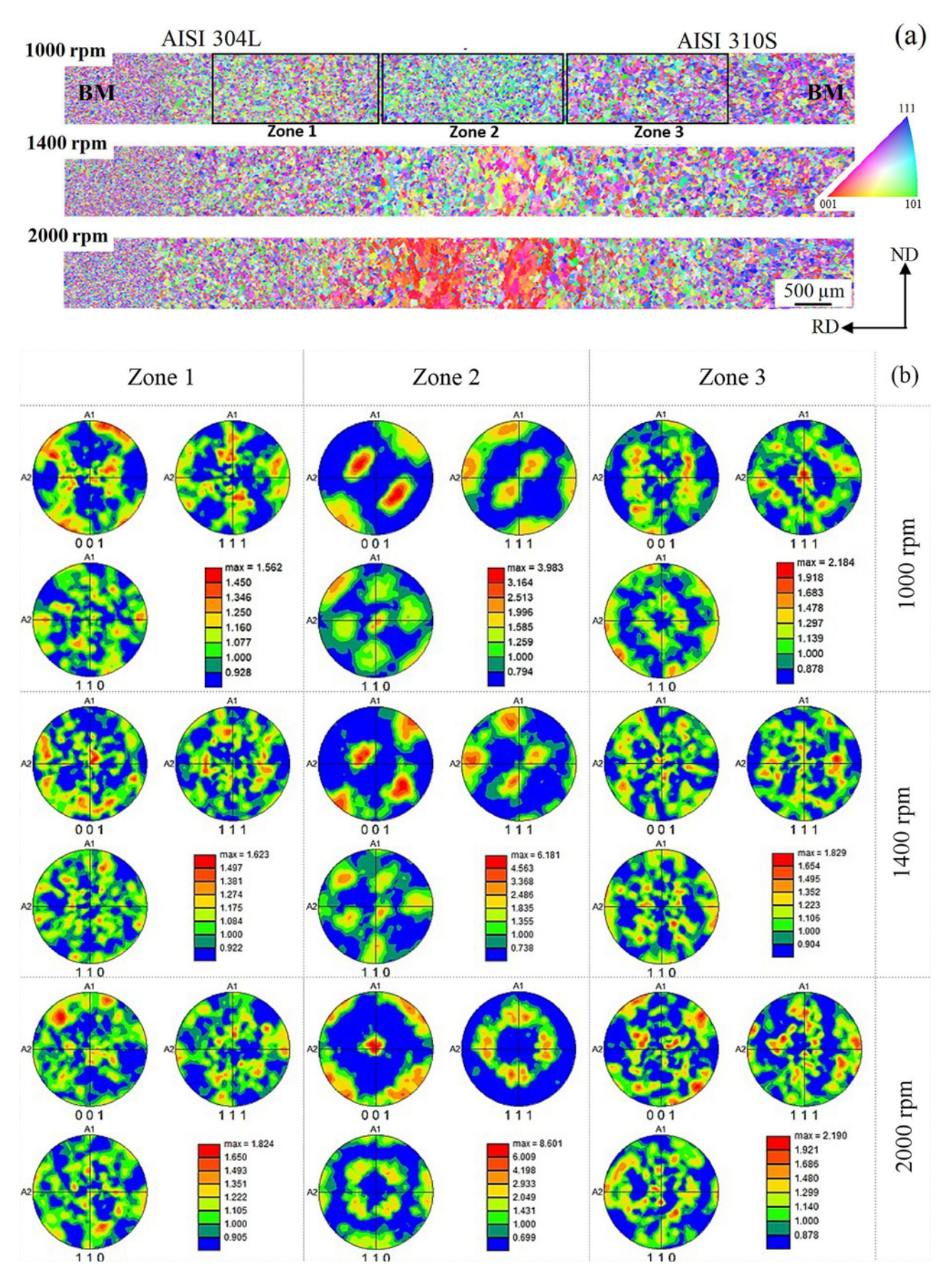


Fig. 7. (a) RD-IPF EBSD maps along the welded joint of the three samples welded by RFW, and (b) pole figures in the welded joint of the three samples welded by RFW under three rotational speeds: 1000 rpm, 1400 rpm, and 2000 rpm.

Table 2. Ultimate tensile strength values of the base metals and the welded samples by RFW under three rotational speeds: 1000 rpm, 1400 rpm, and 2000 rpm

| Sample   | 304L | 310S | 1   | 2   | 3   |  |
|----------|------|------|-----|-----|-----|--|
| Rm (MPa) | 915  | 692  | 320 | 507 | 500 |  |

tary friction welding process.

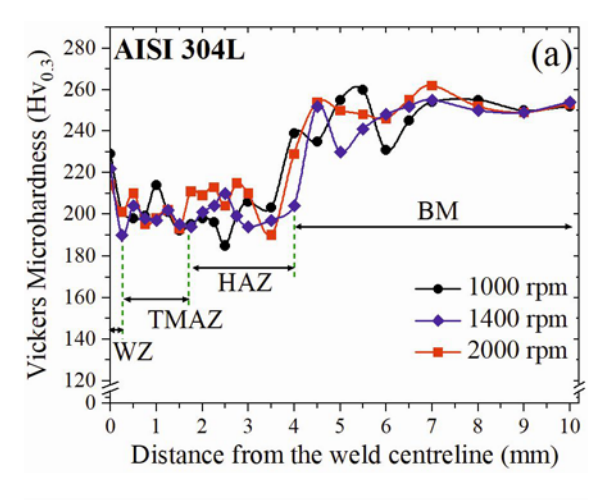
Based on the EBSD results, RFW generates small grains whose crystal orientation evolves as a function of speed, with a majority direction  $<\!100\!>$  // WA for the highest speed. In the adjacent zone, the grains grow, developing the same texture as the small grains, the growth of  $<\!100\!>$  // WA grains appearing preferential. In the thermally affected zones (Zones 1 and 3), there appears, on the one hand, a slight growth of grains (for 2000 rpm, 30  $\mu m$  for 316L steel, and 46  $\mu m$  for 310S) and, on the other hand, the disappearance of the  $<\!111\!>$  // WA fiber texture from the initial states in favor of a quasi-isotropic texture.

#### 3.6. Tensile tests

Tensile tests were conducted on the two base metals and on the three samples welded under varying rotational speeds. Table 2 summarizes the ultimate tensile strength values of the tested samples. It can be seen that 304L stainless steel has the greatest ultimate tensile strength (915 MPa) compared to 310S stainless steel (692 MPa). This difference is mainly due to the difference in grain size between these two base metals, where 304L steel has very fine grains compared to 310S steel. For the ultimate tensile strength values of the welded samples, the joints welded at a rotational speed of 1400 and 2000 rpm have the highest values compared to those welded at a rotational speed of 1000 rpm. Madhappan et al. [20] concluded that tensile tests showed that dissimilar welded joints achieved less strength compared to a similar joint.

#### 3.7. Hardness measurements

The hardness measurements along the welded joint, obtained by varying the rotational speed during RFW of the two different steels, are shown in Fig. 8. It is clear that the difference between the three welded samples is difficult to distinguish, as the curves are interconnected and have a similar appearance. The general appearance of the microhardness curves shows high hardness on the side of 304L stainless steel (Fig. 8a), reaching a value of 250 HV, compared to 310S stainless steel (Fig. 8b), which has a value of 190 HV. The high hardness value of 304L stainless steel can still be attributed to the small grain



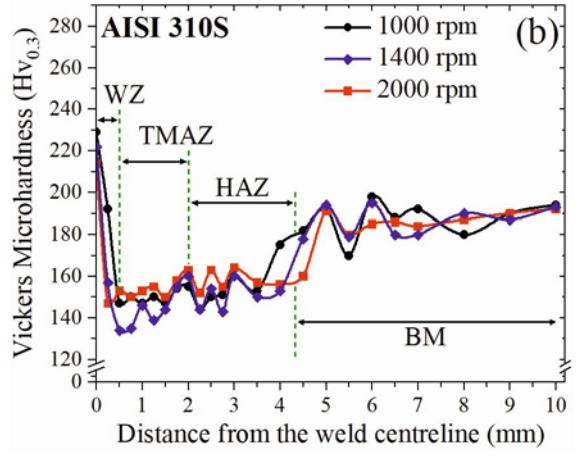


Fig. 8. The Vickers microhardness profiles in the welded joint of: (a) 304L stainless steel to (b) 310S stainless steel after variation of rotational speed during RFW (1000 rpm, 1400 rpm, and 2000 rpm).

size in this material, as confirmed by EBSD analysis and optical microscopy. Additionally, the hardness at the center point of the welded joint has a median hardness (220–230 HV) compared to the maximum values measured in the two dissimilar stainless steels. For the TMAZ, the hardness on the 304L stainless steel side (Fig. 8a) has an average value of 205 HV and an average value of 155 HV on the 310S stainless steel side (Fig. 8b). In contrast, the HAZ of the two different steels has a hardness value almost equal to that of the base metals.

## 4. Conclusions

This investigation aimed to study the effect of rotational speed on the microstructural and mechanical behavior of two dissimilar stainless steels joined by the rotary friction welding. The main results obtained are as follows:

- These two steels were successfully welded by the

rotary friction welding.

- The increase in rotational speed influences the microstructure of the welded joint, with the rotational speed of 2000 rpm presenting a homogeneous microstructure at the interface of the welded joint.
- Based on the EBSD results, friction welding generates small grains whose crystal orientation evolves as a function of speed, with a majority direction  $<\!100\!>$  // WA for the highest speed.
- The welded joint with a rotational speed of 1400 and 2000 rpm has the highest value of ultimate tensile strength.
- Rotary friction welding favored the atomic diffusion through the welded joint of some elements such as iron, chromium, and nickel.

In real industrial practices, these results show that using high rotational speeds (1400–2000 rpm) in rotary friction welding of 304L/310S promotes dynamic recrystallization, resulting in a more uniform microstructure and improved mechanical properties. It provides guidance on selecting the optimal welding parameters for joining various types of stainless steel in high-temperature environments, such as heat exchangers, boilers, and petrochemical pipelines.

#### Acknowledgement

We thank the DGRSDT for its financial contribution to this research work.

#### References

- J. C. Lippold, D. J. Kotecki, Welding Metallurgy and Weldability of Stainless Steels. John Wiley & Sons, New Jersey, 2005. ISBN: 978-0-471-47379-4
- [2] G. F. V. Voort, G. Lucas, E. Manilova, Metallography and microstructures of stainless steels and maraging steels, ASM Handbook 9 (2004) 670–700. https://doi.org/10.31399/asm.hb.v09.a0003767
- [3] M. Sabzi, S. H. Mousavi Anijdan, A. R. Eivani, H. Jafarian, The effect of pulse current changes in PCGTAW on microstructural evolution, drastic improvement in mechanical properties, and fracture mode of dissimilar welded joint of AISI 316L-AISI 310S stainless steels, Mater. Sci. Eng. A 823 (2021) 141700. https://doi.org/10.1016/j.msea.2021.141700
- [4] N. V. Amudarasan, K. Palanikumar, K. Shanmugam, Tensile and impact properties of AISI 304L stainless steel welded joints using austenitic and duplex stainless steel filler metal, Int. J. Eng. Res. Technol. (IJERT) 1 (2012) 1–5. <a href="https://doi.org/10.17577/IJERTV1IS9295">https://doi.org/10.17577/IJERTV1IS9295</a>
- [5] T. Amaro Vicente, L. A. Oliveira, E. O. Correa, R. P. Barbosa, V. B. P. Macanhan, N. G. de Alcântara, Stress corrosion cracking behaviour of dissimilar welding of AISI 310S austenitic stainless steel to 2304 duplex stainless steel, Metals 8 (2018) 195. https://doi.org/10.3390/met8030195

- [6] T. M. Mower, M. J. Long, Mechanical behavior of additive manufactured, powder-bed laser-fused materials, Mater. Sci. Eng. A 651 (2016) 198–213. https://doi.org/10.1016/j.msea.2015.10.068
- [7] W. E. Luecke, J. A. Slotwinski, Mechanical properties of austenitic stainless steel made by additive manufacturing, J. Res. Natl. Inst. Stand. Technol. 119 (2014) 398–418. <a href="http://dx.doi.org/10.6028/jres.119.015">http://dx.doi.org/10.6028/jres.119.015</a>
- [8] A. Bahrami, S. M. Rafiaei, M. Yazdan Mehr, Root cause analysis of failure in superheater tubes in a power plant, Metallogr. Microstruct. Anal. 8 (2019) 275–280.
- https://doi.org/10.1007/s13632-019-00533-4
  [9] N. Özdemir, F. Sarsilmaz, A. Hasçalik, Effect of ro-
- [9] N. Ozdemir, F. Sarsilmaz, A. Hasçalik, Effect of rotational speed on the interface properties of friction-welded AISI 304L to 4340 steel, Mater. Des. 28 (2007) 301–307.
  - https://doi.org/10.1016/j.matdes.2005.06.011
- [10] V. V. Satyanarayana, G. Madhusudhan Reddy, T. Mohandas, Dissimilar metal friction welding of austenitic-ferritic stainless steels, J. Mater. Process. Technol. 160 (2005) 128–137. https://doi.org/10.1016/j.jmatprotec.2004.05.017
- [11] P. Sathiya, S. Aravindan, A. Noorul Haq, Some experimental investigations on friction welded stainless steel joints, Mater. Des. 29 (2008) 1099–1109. https://doi.org/10.1016/j.matdes.2007.06.006
- [12] J. A. James, R. Sudhish, Study on the effect of interlayer in friction welding for dissimilar steels: SS 304 and AISI 1040, Proc. Technol. 25 (2016) 1191–1198. https://doi.org/10.1016/j.protcy.2016.08.238
- [13] W. Li, A. Vairis, M. Preuss, T. Ma, Linear and rotary friction welding review, Int. Mater. Rev. 61 (2016) 71–100. https://doi.org/10.1080/09506608.2015.1109214
- [14] M. Maalekian, Friction welding critical assessment of literature, Sci. Technol. Weld. Join. 12 (2007) 738– 759. https://doi.org/10.1179/174329307X249333
- [15] M. B. Uday, M. N. A. Fauzi, H. Zuhailawati, A. B. Ismail, Advances in friction welding process: A review, Sci. Technol. Weld. Join. 15 (2010) 534–558. https://doi.org/10.1179/136217110X12785889550064
- [16] G. B. Sathishkumar, P. Sethuraman, C. Chanakyan, S. Sundaraselvan, A. Joseph Arockiam, S. V. Alagarsamy, A. Elmariung, M. Meignanamoorthy, M. Ravichandran, S. Jayasathyakawin, Friction welding of similar and dissimilar materials: A review, Mater. Today. Proc. 81 (2023) 208–211. https://doi.org/10.1016/j.matpr.2021.03.089
- [17] N. K. Mishra, A. Shrivastava, Improvement in strength and ductility of rotary friction welded Inconel 600 and stainless steel 316L with Cu interlayer, CIRP J. Manuf. Sci. Technol. 41 (2023) 19–29. <a href="https://doi.org/10.1016/j.cirpj.2022.12.006">https://doi.org/10.1016/j.cirpj.2022.12.006</a>
- [18] W. Cai, G. Daehn, J. Li, R. Mishra, A. Vivek, H. Khan, M. Komarasamy, A state-of-the-art review on solid-state metal joining, J. Manuf. Sci. Eng. 141 (2019) 031012. <a href="https://doi.org/10.1115/1.4041182">https://doi.org/10.1115/1.4041182</a>
- [19] Z. Boumerzoug, E. Priymak, A. Stepanchukova, A. Helbert, F. Brisset, T. Baudin, Texture of rotary-friction-welded from dissimilar medium carbon steels, World J. Condens. Matter. Phys. 10 (2020) 178–190. https://doi.org/10.4236/wjcmp.2020.104011
- [20] D. K. Madhappan, P. K. Palani, M. Arulraj, Dissimilar welding of UNS S31803 and UNS S30400 tubes superiority and adverse in rotary friction welding, Proc.

- [21] A. Atamashkin, E. Priyma, E. Tulibaev, Y. Syomka, V. Trushov, Influence of force parameters of rotary friction welding on the microstructure and mechanical properties of welded joints of high-strength drill pipes, Int. J. Interact. Des. Manuf. (2024). https://doi.org/10.21203/rs.3.rs-4332323/v1
- [22] A. A. Mattie, S. Y. Ezdeen, G. I. Khidhir, Optimization of parameters in rotary friction welding process of dissimilar austenitic and ferritic stainless steel using finite element analysis, Adv. Mech. Eng. 15 (2023). <a href="https://doi.org/10.1177/16878132231186">https://doi.org/10.1177/16878132231186</a>
- [23] M. D. Kumar, P. K. Palani, Characterization studies on weld strength of rotary friction welded austenitic stainless steel tubes, Mater. Today Proc. 41 (2021) 1024–1029.
  - https://doi.org/10.1016/j.matpr.2020.06.383
- [24] J. S. Chatha, A. Handa, T. S. Bedi, Strength analysis of rotary friction welded joints of dissimilar steel grades, Mater. Today Proc. 38 (2021) 242–247. https://doi.org/10.1016/j.matpr.2020.07.090
- [25] M. Kimura, A. Ichihara, M. Kusaka, et al. Joint properties and their improvement of AISI 310S austenitic stainless steel thin walled circular pipe friction welded joint, Mater. Des. 38 (2012) 38–46. <a href="https://doi.org/10.1016/j.matdes.2012.02.006">https://doi.org/10.1016/j.matdes.2012.02.006</a>
- [26] G. Wang, J. Li, J. Xiong, W. Zhou, F. Zhang, Study on microstructure evolution of AISI 304 stainless steel joined by rotary friction welding, Weld. World 62 (2018) 1187–1193. https://doi.org/10.1007/s40194-018-0613-7
- [27] K. H. Lo, C. H. Shek, J. K. L. Lai, Recent developments in stainless steels, Mater. Sci. Eng. R: Reports 65 (2009) 39–104. https://doi.org/10.1016/j.mser.2009.03.001
- [28] A. H. Saedi, E. Hajjari, S. M. Sadrossadat, Microstructural characterization and mechanical properties of TIG-welded API 5L X60 HSLA steel and AISI 310S stainless steel dissimilar joints, Metall. Mater. Trans. A 49 (2018) 5497–5508. https://doi.org/10.1007/s11661-018-4890-y

C. Jiang, Effect of rotation speed on microstructure and mechanical properties of continuous drive friction welded dissimilar joints of 6061-T6 Al and copper, Metals 12 (2022) 1173. https://doi.org/10.3390/met12071173

[29] X. Zhu, Y. Fan, L. Xie, X. Xiao, P. Wang, S. Yang,

- [30] A. R. Beeravolu, N. K. Babu, M. K. Talari, A. U. Rehman, P. Srirangam, Influence of microstructure and mechanical properties of dissimilar rotary friction welded Inconel to stainless steel joints, Materials 16 (2023) 3049. https://doi.org/10.3390/ma16083049
- [31] S. Celik, I. Ersozlu, Dynamic recrystallization of friction welded AISI 316 stainless steel joints, Mater. Test. 62 (2020) 1126–1130.
   <a href="https://doi.org/10.3139/120.111600">https://doi.org/10.3139/120.111600</a>
- [32] V. A. Alza, Rotational friction welding in dissimilar steels AISI 1018-AISI 2225: Effects on hardness, fatigue and microstructure, IOSR J. Mech. Civ. Eng. 19 (2022) 37–39. <a href="https://doi.org/10.9790/1684-1903023749">https://doi.org/10.9790/1684-1903023749</a>
- [33] H. Purwanto, Interface structure in friction welded joints between stainless steel 304 and mild carbon steel, J. Chem. Process. Mater. Technol. 1 (2022) 8– 14. http://dx.doi.org/10.36499/jcpmt.v1i1.5881
- [34] H. Firmanto, S. Candra, M. A. Hadiyat, Y. P. Triastomo, I. Wirawan, Tensile strength and microstructure of rotary-friction-welded carbon-steel and stainless-steel joints, J. Manuf. Mater. Process. 7 (2023) 7. <a href="https://doi.org/10.3390/jmmp7010007">https://doi.org/10.3390/jmmp7010007</a>
- [35] E. Y. Priymak, M. L. Lobanov, S. V. Belikov, M. S. Karabanalov, I. L. Yakovleva, Structure formation patterns and crystallographic texture in welded joints of medium-carbon alloy steels in the process of rotary friction welding, Phys. Metals Metallogr. 123 (2022) 559–566.
  - https://doi.org/10.1134/S0031918X22060126